



Early Gamma Oscillations Synchronize Developing Thalamus and Cortex

Marat Minlebaev, *et al.*
Science **334**, 226 (2011);
DOI: 10.1126/science.1210574

This copy is for your personal, non-commercial use only.

If you wish to distribute this article to others, you can order high-quality copies for your colleagues, clients, or customers by [clicking here](#).

Permission to republish or repurpose articles or portions of articles can be obtained by following the guidelines [here](#).

The following resources related to this article are available online at www.sciencemag.org (this information is current as of October 13, 2011):

Updated information and services, including high-resolution figures, can be found in the online version of this article at:

<http://www.sciencemag.org/content/334/6053/226.full.html>

Supporting Online Material can be found at:

<http://www.sciencemag.org/content/suppl/2011/10/13/334.6053.226.DC1.html>

This article **cites 28 articles**, 13 of which can be accessed free:

<http://www.sciencemag.org/content/334/6053/226.full.html#ref-list-1>

Early Gamma Oscillations Synchronize Developing Thalamus and Cortex

Marat Minlebaev,^{1,2} Matthew Colonnese,^{1,2} Timur Tsintsadze,^{1,2}
Anton Sirota,^{3*} Roustem Khazipov^{1,2*†}

During development, formation of topographic maps in sensory cortex requires precise temporal binding in thalamocortical networks. However, the physiological substrate for such synchronization is unknown. We report that early gamma oscillations (EGOs) enable precise spatiotemporal thalamocortical synchronization in the neonatal rat whisker sensory system. Driven by a thalamic gamma oscillator and initially independent of cortical inhibition, EGOs synchronize neurons in a single thalamic barreloid and corresponding cortical barrel and support plasticity at developing thalamocortical synapses. We propose that the multiple replay of sensory input in thalamocortical circuits during EGOs allows thalamic and cortical neurons to be organized into vertical topographic functional units before the development of horizontal binding in adult brain.

Sensory cortex is organized as a topographic map consisting of arrays of columns that each receive an input from a particular region of sensory space (1). In the rodent “barrel” cortex, each cortical barrel column receives a specific input, conveyed via the thalamus, from a

corresponding whisker (2). Development of the topographic thalamocortical connections depends critically on activity driven by the whiskers (2–4). During development, sensory input triggers various cortical activity patterns (5–8). However, it remains unknown how the sensory input from a

single whisker is processed in the corresponding developing cortical column.

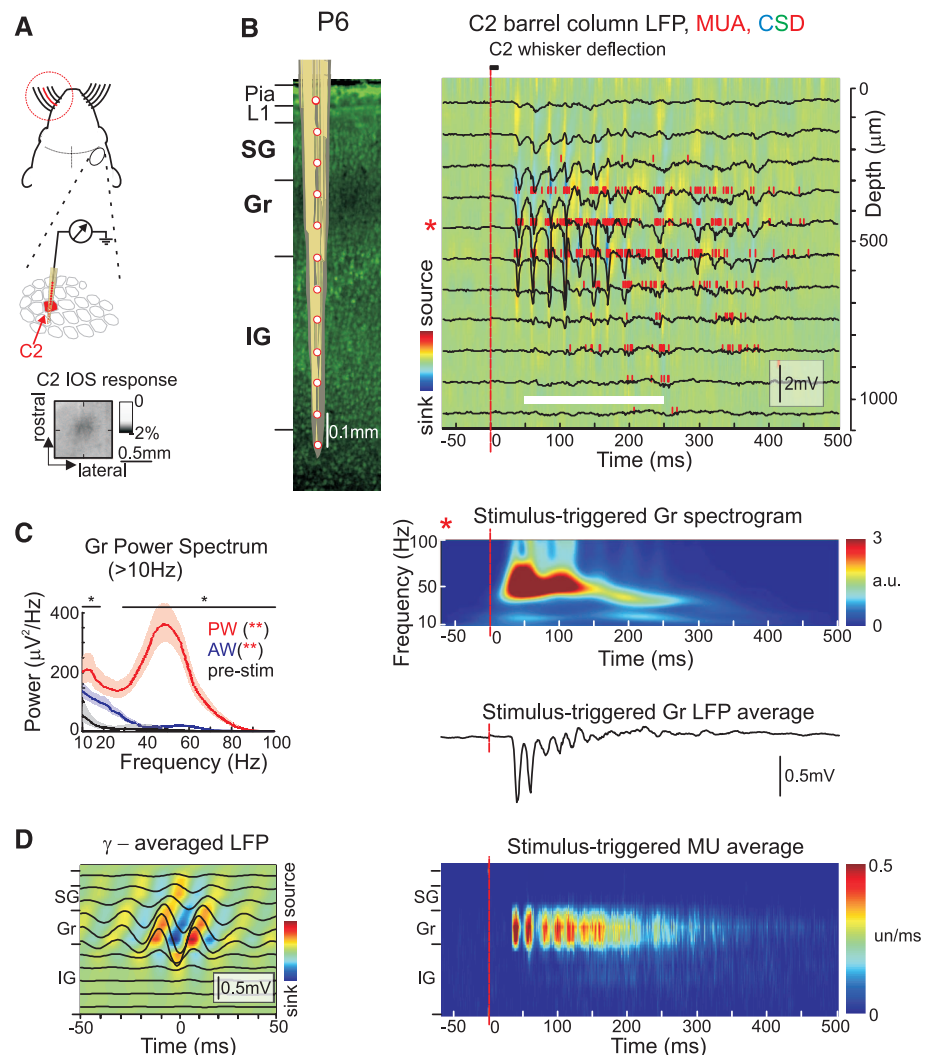
We found that in postnatal days 2 to 7 (P2 to P7), rats brief single principal whisker (PW) deflections evoke an oscillatory local field potential (LFP) response in the gamma band in the corresponding cortical barrel (peak frequency 55 ± 2 Hz; $n = 45$ rats) (Fig. 1 and fig. S1). Multiunit activity (MUA), gamma oscillation power, and the current sinks of these early gamma oscillations (EGOs) were maximal in the granular (Gr) layer (Fig. 1, B to D, and Fig. 2C). EGOs were time-locked to the stimulus and were apparent in the stimulus-triggered average LFP and MUA time histograms (Fig. 1B). Gr MUA was strongly phase-modulated by EGOs and occurred during the descending phase and troughs of gamma

¹INSERM U901, 163 Avenue de Luminy, B.P. 13, 13273 Marseille, France. ²Université Aix-Marseille, 163 Avenue de Luminy, 13273 Marseille, France. ³University of Tuebingen Center for Integrative Neuroscience, Paul-Ehrlich Strasse 15, Tuebingen 76072, Germany.

*These authors contributed equally to this work.

†To whom correspondence should be addressed. E-mail: khazipov@inmed.univ-mrs.fr

Fig. 1. Brief single-whisker deflection evokes gamma oscillations in the corresponding cortical barrel of a P6 neonatal rat. **(A)** Scheme of the experimental setup, with principal barrel location detected by intrinsic optical signal imaging (IOS) shown below. **(B)** (Top left) Recording sites of a multielectrode array overlaid on a Ctip2-stained cortical slice. IG, infragranular. (Top right) Sensory response evoked by C2 PW stimulation at different depths of the C2 cortical barrel column. LFP, black traces; MUA, red bars overlaid on color-coded current-source density (CSD) plot. (Bottom) The stimulus-triggered averages ($n = 100$) for Gr layer (red asterisk) wavelet spectrogram, average Gr layer LFP, and MUA peristimulus time histograms (PSTHs) across layers. **(C)** Power spectral density of Gr layer LFP during a 200-ms time window [white horizontal bar in (B)] following PW or AW sensory evoked potential (SEP) or during a prestimulus epoch. Shading and error bars hereafter show jackknife standard deviation. **(D)** Gamma-trough triggered average Gr LFP and CSD map.



cycles (figs. S1 and S2C). Day-by-day analysis revealed that power in the gamma band increased from birth to attain maximal values at P2 to P7 and abruptly declined at P8, followed by a gradual increase both in spontaneous and sensory-evoked activity in the gamma frequency range (Fig. 2D and figs. S1 and S3). Simultaneous recordings in Gr layer of two neighboring barrel columns revealed that EGOs are restricted to the principal barrel ($n = 13$) (P5 to P7) (Fig. 2, A, C, and D, and fig. S2).

We further addressed the development of activity transfer from Gr to the downstream supragranular (SG) layers and of horizontal synchronization by gamma oscillations in the neighboring columns. During the first postnatal week, PW-evoked responses in SG layers were weak and virtually no response was seen to adjacent whisker (AW) stimulation in either Gr or SG layers (Fig. 1, Fig. 2, A, C, and E, and fig. S2). This is in keeping with the emergence of suprathreshold Gr to SG and horizontal connections only from the second postnatal week (9, 10). From the end of the second postnatal week onward, power in the gamma frequency band in Gr and SG layers progressively increased (Fig. 2E and fig. S3), and gamma oscillations started to synchronize units in the neighboring columns (fig. S2). Unlike EGOs, these later-emerging “adult” gamma oscillations were not time-locked to the stimulus

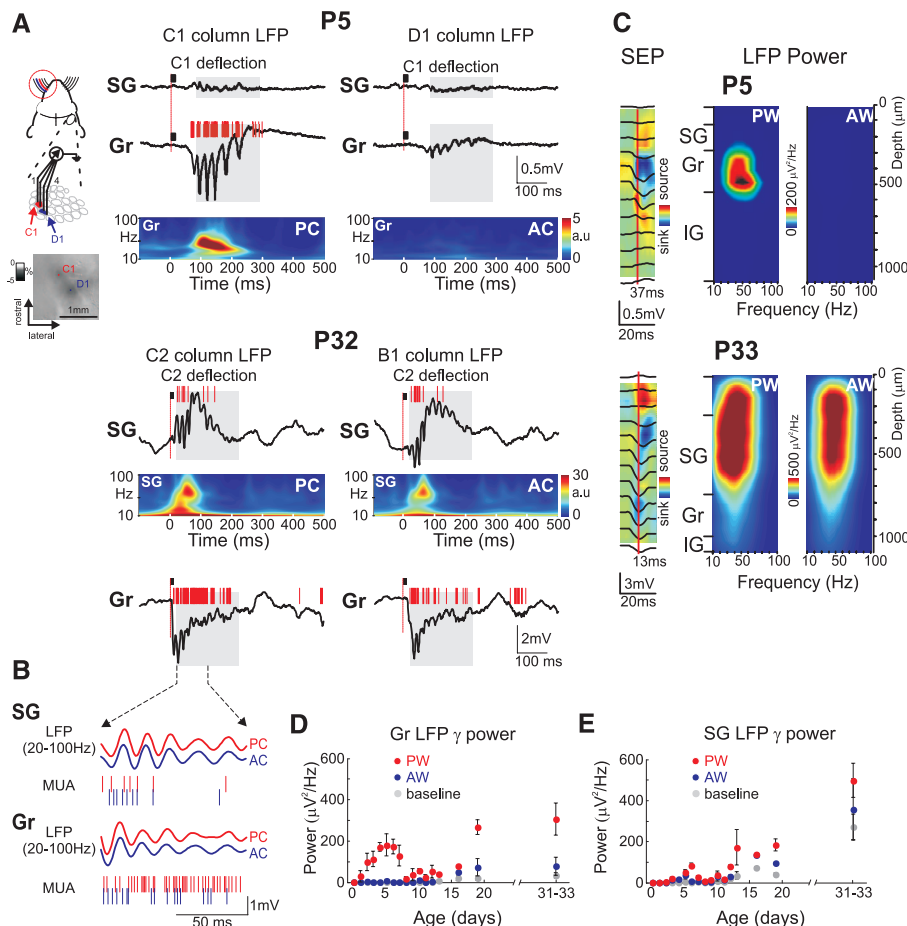
and were maximal in SG layers. Simultaneous recordings from neighboring barrel columns in P19 to P33 rats ($n = 6$) revealed strong horizontal gamma synchronization of units (Fig. 2, A and B, and fig. S2). Thus, during development, sensory-evoked gamma activity switches from transient input-specific “vertical” EGOs to “horizontal” gamma oscillations synchronizing activity in neighboring cortical columns. The switch is characterized by a developmental gap between these two forms of gamma activity: EGOs disappear around P8, whereas adult gamma activity gradually builds up along with a development of the active cortical state, manifested by an increase in background activity (Fig. 2, D and E, and figs. S1 and S3) (8, 11, 12) and with the development of explorative behaviors and active whisking that starts at P11 to P13 (13). That EGOs are local and are barely seen at the cortical surface may explain an apparent contradiction to the generally accepted idea, based on scalp electroencephalogram recordings, that gamma oscillations emerge relatively late in development (14, 15).

The existence of robust EGOs during the neonatal period is surprising because feed-forward perisomatic inhibition, known to be central for the generation of cortical gamma oscillations (15–19), is not present in Gr layer until P6 to P7 (20, 21). Using whole-cell recordings, we found that in all Gr neurons recorded between P2 and

P7 ($n = 30$), PW stimulation evokes stimulus-locked gamma-rhythmic excitatory postsynaptic currents (EPSCs) tightly locked to the field EGO’s troughs (Fig. 3A and fig. S4, A and B). These gamma-rhythmic EPSCs were not present in P10 to P11 rats ($n = 3$), in agreement with the disappearance of field EGOs after P8. The engagement of inhibitory circuits into EGOs followed a different age-dependent track. At P2 to P3, only three of five cells displayed any inhibitory postsynaptic currents (IPSCs), and these occurred at the end of EGOs. By P5 to P7, IPSCs showed gamma rhythmicity during EGOs (Fig. 3, A and B, and fig. S4, A and B), which was also reflected in firing pattern and gamma-rhythmic EPSCs in a fast-spiking interneuron at P7 (fig. S5). Cells in SG layers received only weak and largely sub-threshold excitatory input during the first postnatal week. In contrast, at P19 to P20, SG neurons were activated during gamma oscillations, and the gamma rhythmicity of IPSCs was superior to that of EPSCs, a reversal from earlier ages ($n = 5$ cells) (Fig. 3B and fig. S4, C and D) (22, 23).

In keeping with the whole-cell data, which suggested a limited contribution of IPSCs to EGOs in the youngest animals, blockade of cortical inhibition by gabazine did not modify EGOs at P2 to P4 ($n = 5$) but strongly reduced them at P6 ($n = 4$) (Fig. 3, E and F). Thus, EGOs primarily result from a gamma-rhythmic excitatory input to

Fig. 2. Developmental switch from input-specific early gamma oscillations to horizontal adult gamma oscillations. **(A)** IOS-guided multishank recordings of responses evoked by a single-whisker deflection in SG and Gr layers of the principal and adjacent barrel columns in a P5 (top traces) and P32 (bottom traces) rat. Color-contour plots show stimulus-triggered averages for Gr (P5) and SG (P19) LFP wavelet spectrograms. **(B)** Expanded gamma-filtered (20- to 100-Hz bandpass) LFP and MUA in SG and Gr layers for the principal column (PC, red) and adjacent column (AC, blue) to a single-whisker deflection recorded simultaneously at P32. **(C)** PW deflection evoked averaged sensory potentials overlaid on a color CSD map (left, red vertical lines indicate the time of the stimulus onset) and mean power spectrum of the PW (middle) and AW (right) evoked responses throughout the cortical depth in a P5 (top) and P33 (bottom) rat. **(D)** and **(E)** Postnatal changes in PW-evoked (red), AW-evoked (blue), and baseline (gray) gamma power (peak between 40 and 60 Hz in 200-ms window) in Gr (D) and SG (E) layers. Pooled data from 67 rats.



Gr cells, which constitutes the only drive for EGOs during the first postnatal days. Local inhibitory circuits are progressively recruited into EGOs only at the end of the first postnatal week.

In agreement with previous results from thalamocortical slices (20, 21), the onset of PW-

evoked IPSCs was delayed by >100 ms from the onset of EPSCs at P2 to P3. This temporal “integration window” rapidly shortened during the first postnatal week (Fig. 3, C and D) to attain 5.9 ± 1.5 ms ($n = 6$) at P7 to P11 [compared with ~ 1 ms in adults (24)]. Accordingly, suppression of

Gr units after the first peak in stimulus-triggered MUA histogram (dip) was unchanged at P2 to P4 ($n = 5$) but was strongly reduced at P6 ($n = 4$) after blockade of cortical inhibition (Fig. 3, E and G). Thus, the two facets of perisomatic inhibition—feed-forward inhibition and gamma synchronization—show remarkably similar developmental profiles during the first postnatal week.

Simultaneous recordings from topographically aligned loci in the ventral posterior medial (VPM) nucleus of the thalamus and corresponding cortical column ($n = 9$) (P5 to P7) (Fig. 4A) revealed PW-evoked gamma-rhythmic VPM MUA responses (peak frequency 48 ± 1 Hz), strongly coherent with cortical EGOs (Fig. 4, B to E). Thalamic units showed strong phase modulation relative to the cortical EGOs (resultant vector = 0.24) such that they fired 7 ± 1 ms ahead of Gr cells (Fig. 4, D and E). This thalamocortical binding was maintained for eight EGO cycles, indicating a multiple replay of a sensory input in topographic thalamocortical microcircuits (Fig. 4F). Interestingly, blockade of intrathalamic inhibition suppressed cortical EGOs at P2 to P4 ($n = 5$) (fig. S9), suggesting that the generation of thalamic gamma activity involves synchronization driven by the reticular nucleus (25).

Our findings suggest the following network model (Fig. 4G). Sensory input from a whisker activates an inhibition-based gamma oscillator in the thalamic barreloid, which imposes topographic feed-forward synchronization in the corresponding cortical barrel (Fig. 4G, 1) (26, 27). Cortical interneurons then become involved in EGOs in an age-dependent manner (Fig. 4G, 2). Until \sim P5, EGOs are independent of cortical inhibition. Starting from P5, along with the development of feed-forward inhibition, interneurons are recruited and support EGOs by controlling runaway recurrent cortical excitation. Thus, during the first postnatal week, EGOs undergo evolution from a primitive form of cortical activity passively following a thalamic oscillator, to a more complex interactive model in which an active cortical oscillator, by virtue of emerging inhibition, starts to support gamma oscillations.

The first postnatal week is also characterized by an enhanced plasticity of thalamocortical connections (28). From a synaptic plasticity standpoint, EGOs provide repetitive synchronization of thalamic and cortical neurons, thus creating conditions for potentiation of the topographic thalamocortical connections (29). Indeed, 30 artificial EGOs (aEGOs), mimicked by pairing sub-threshold gamma-rhythmic (50 Hz) thalamic input with action potentials in Gr neurons in thalamocortical slices, resulted in long-lasting potentiation of thalamocortical EPSPs by $23 \pm 1\%$ ($n = 9$) (P4 to P6) (Fig. 4H). In contrast, 30 artificial spindle-bursts (10 Hz) or rhythmic pairing at 0.5 Hz induced a depression or no change in EPSPs, respectively (Fig. 4H).

In summary, we show that EGOs are a characteristic activity pattern transiently expressed in the developing rat barrel cortex during the critical

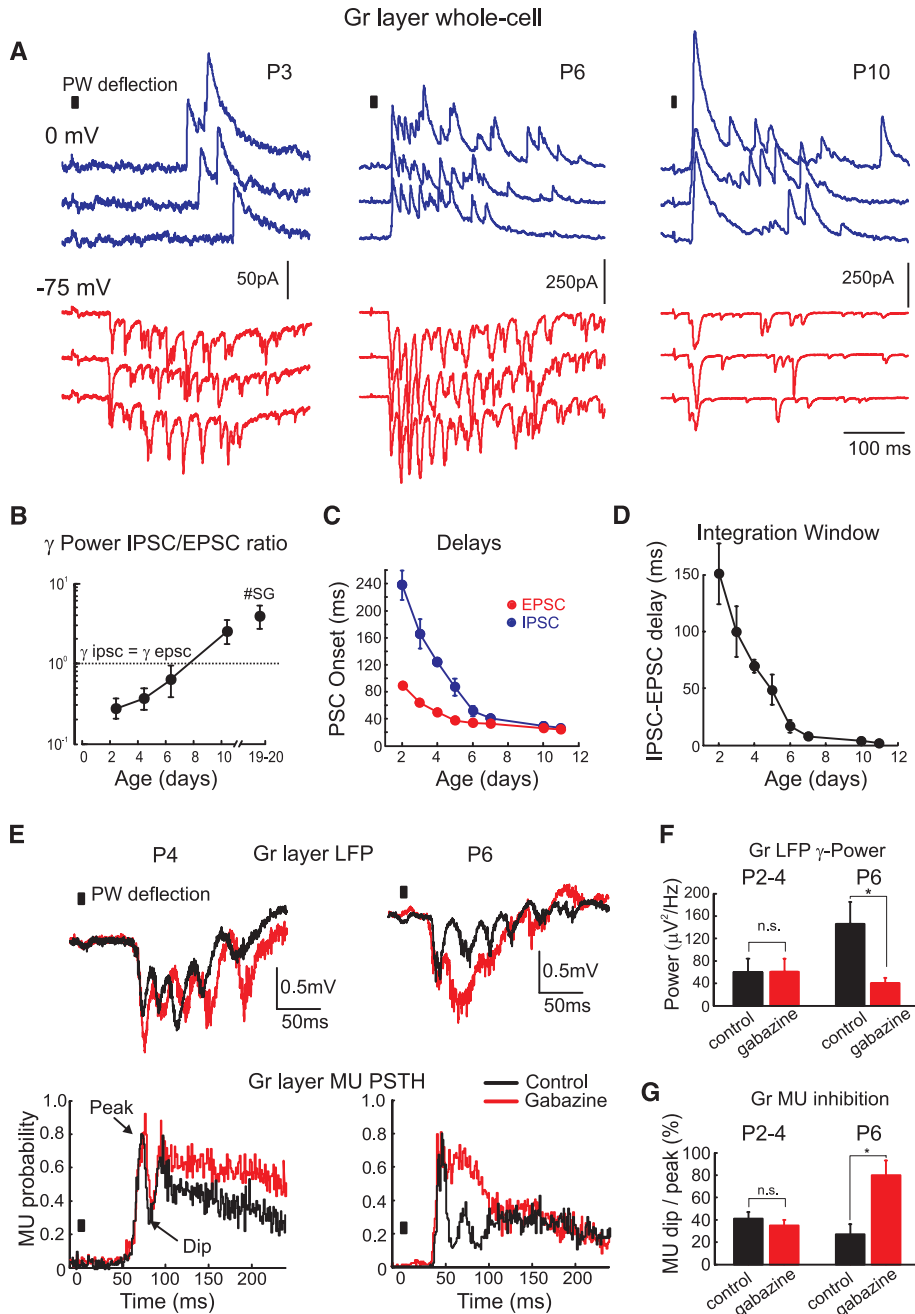
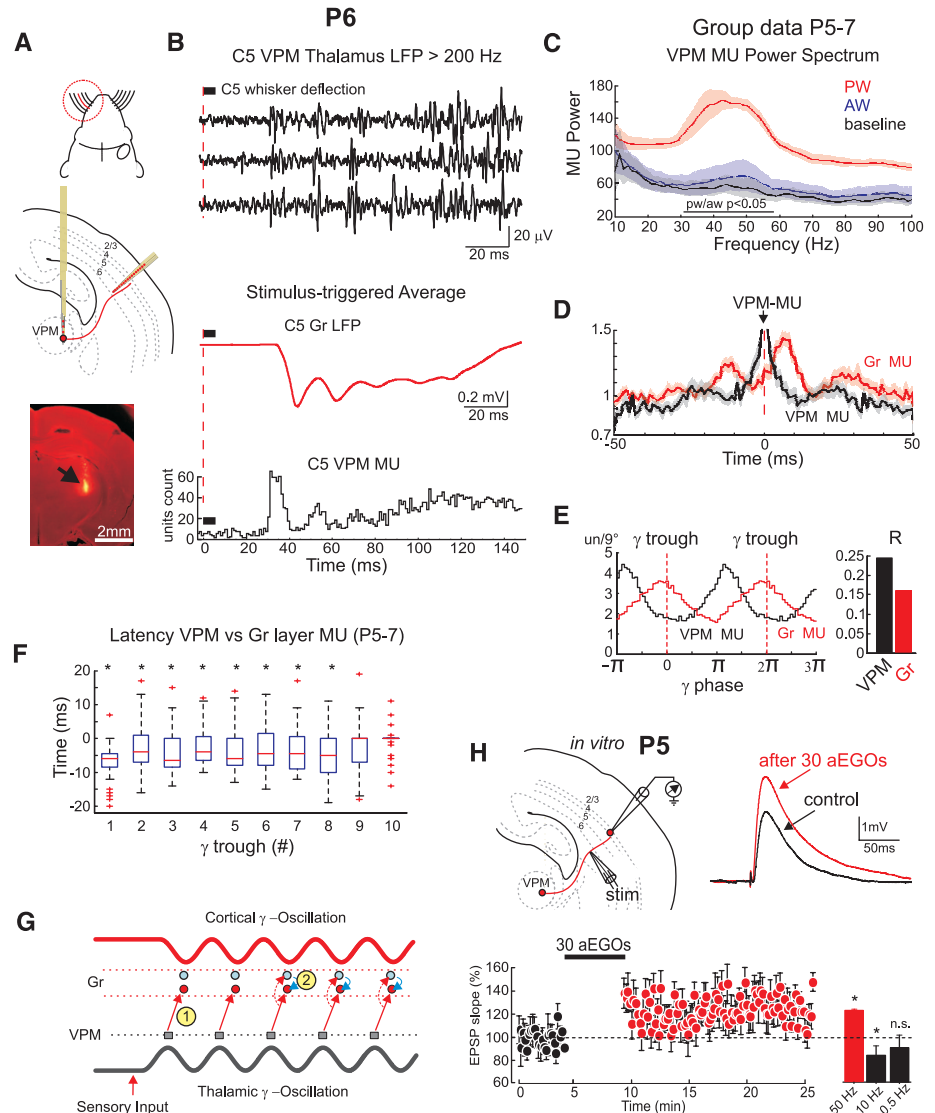


Fig. 3. Synaptic mechanisms of early gamma oscillations. (A) Whole-cell responses evoked by PW stimulation in Gr neurons at different ages recorded in voltage clamp to separate IPSCs (blue top traces at 0 mV) and EPSCs (red bottom traces at -75 mV). (B) Age dependence of the IPSC/EPSC gamma power ratio in Gr cells (P2 to P11) ($n = 33$ cells) and SG cells (P19 to P20) ($n = 5$ cells). (C) Age dependence of EPSCs and IPSCs onset delay in Gr cells from PW stimulus onset. (D) Age dependence of the integration window, defined as the difference between EPSCs and IPSCs onset delay. (E) (Top) PW-evoked Gr LFP responses in P4 and P6 rats before (black traces) and after (red traces) epipial application of the γ -aminobutyric acid type A receptor blocker gabazine ($50 \mu M$). (Bottom) Corresponding Gr MUA PSTHs. (F and G) Summary plots of the effects of gabazine on (F) PW-evoked Gr LFP gamma power at P2 to P4 ($n = 5$) and P6 ($n = 4$), and (G) MUA dip-to-peak ratio [as shown in (E)].

Fig. 4. Thalamocortical binding during early gamma oscillations. **(A)** (Top) Experimental setup for simultaneous recordings of single-whisker evoked responses in the corresponding VPM barreloid and cortical barrel column. (Bottom) A coronal section showing the location of the Dil-labeled recording electrode (arrow). **(B)** (Top) Three sequential responses to C5 whisker deflections in the C5 barreloid of VPM thalamus. (Bottom) Average Gr layer LFP (red) and VPM MUA PSTH (black histogram) from 100 deflections on the same time scale. **(C)** Power spectral density for VPM MUA evoked by PW and AW stimulations and for baseline activity. **(D)** Autocorrelogram for PW-evoked VPM units and cross-correlogram for Gr versus VPM units. **(E)** Cortical gamma-phase modulation of Gr and VPM units and the Rayleigh's resultant vectors (R). **(F)** Latency in VPM versus Gr layer MUA for each consecutive cycle of the PW-evoked EGO. [(C) to (F) show pooled data from nine P5 to P7 rats.] **(G)** Proposed network EGOs model. **(H)** (Top left) Scheme of whole-cell recordings of thalamocortical EPSPs in thalamocortical slices. (Top right) Subthreshold EPSPs in Gr neurons (control, black trace) were potentiated after 30 episodes of artificial EGO-like pairing of thalamic inputs with spikes in postsynaptic neurons (after pairing, red trace). (Bottom) Time course (left) and averages (\pm SE) (right) of normalized EPSP slopes after 150 pairings, organized in 30 aEGOs (50 Hz), 30 spindle bursts (10 Hz), and rhythmic pairing at 0.5 Hz ($n = 9$ P4 to P6 cells for each condition).



period for activity-dependent plasticity in thalamocortical synapses. In contrast to the inhibition-based “adult” gamma oscillations that emerge at the end of the second postnatal week and enable horizontal synchronization, EGOs are primarily driven by gamma-rhythmic excitatory thalamic input and provide vertical synchronization between topographically aligned thalamic and cortical neurons. Multiple replay of sensory input in the thalamocortical synapses during EGOs (“repetitio est mater studiorum”) may allow thalamic and cortical neurons to be woven into vertical topographic functional units before the development of horizontal binding and other integrative cortical functions (14–19) subserved by “adult” gamma oscillations in mature brain.

References and Notes

1. V. B. Mountcastle, *J. Neurophysiol.* **20**, 408 (1957).
2. H. Van der Loos, T. A. Woolsey, *Science* **179**, 395 (1973).
3. K. Fox, *J. Neurosci.* **12**, 1826 (1992).
4. D. J. Simons, P. W. Land, *Nature* **326**, 694 (1987).
5. R. Khazipov *et al.*, *Nature* **432**, 758 (2004).

6. M. Minlebaev, Y. Ben-Ari, R. Khazipov, *J. Neurophysiol.* **97**, 692 (2007).
7. J. W. Yang, I. L. Hanganu-Opatz, J. J. Sun, H. J. Luhmann, *J. Neurosci.* **29**, 9011 (2009).
8. M. T. Colonnese *et al.*, *Neuron* **67**, 480 (2010).
9. I. Bureau, G. M. Shepherd, K. Svoboda, *Neuron* **42**, 789 (2004).
10. A. J. Borgdorff, J. F. Poulet, C. C. Petersen, *J. Neurophysiol.* **97**, 2992 (2007).
11. P. Golshani *et al.*, *J. Neurosci.* **29**, 10890 (2009).
12. N. L. Rochefort *et al.*, *Proc. Natl. Acad. Sci. U.S.A.* **106**, 15049 (2009).
13. M. Landers, H. Philip Zeigler, *Somatosens. Mot. Res.* **23**, 1 (2006).
14. P. J. Uhlhaas, F. Roux, E. Rodriguez, A. Rotarska-Jagiela, W. Singer, *Trends Cogn. Sci.* **14**, 72 (2010).
15. M. A. Whittington, M. O. Cunningham, F. E. LeBeau, C. Racca, R. D. Traub, *Dev. Neurobiol.* **71**, 92 (2011).
16. P. Fries, *Annu. Rev. Neurosci.* **32**, 209 (2009).
17. G. Buzsaki, *Rhythms of the Brain* (Oxford Univ. Press, Oxford, 2006).
18. M. Bartos, I. Vida, P. Jonas, *Nat. Rev. Neurosci.* **8**, 45 (2007).
19. X. J. Wang, *Physiol. Rev.* **90**, 1195 (2010).
20. A. Agmon, D. K. O’Dowd, *J. Neurophysiol.* **68**, 345 (1992).
21. M. I. Daw, M. C. Ashby, J. T. Isaac, *Nat. Neurosci.* **10**, 453 (2007).

22. A. Hasenstaub *et al.*, *Neuron* **47**, 423 (2005).
23. B. V. Atallah, M. Scanziani, *Neuron* **62**, 566 (2009).
24. L. Gabernet, S. P. Jadhav, D. E. Feldman, M. Carandini, M. Scanziani, *Neuron* **48**, 315 (2005).
25. D. Pinault, M. Deschênes, *Neuroscience* **51**, 245 (1992).
26. I. Timofeev, M. Steriade, *J. Physiol.* **504**, 153 (1997).
27. M. Castelo-Branco, S. Neunschwander, W. Singer, *J. Neurosci.* **18**, 6395 (1998).
28. D. E. Feldman, R. A. Nicoll, R. C. Malenka, *J. Neurobiol.* **41**, 92 (1999).
29. Y. Dan, M. M. Poo, *Physiol. Rev.* **86**, 1033 (2006).

Supporting Online Material

www.sciencemag.org/cgi/content/full/334/6053/226/DC1
 Materials and Methods
 Figs. S1 to S10
 References

1 July 2011; accepted 1 September 2011
 10.1126/science.1210574